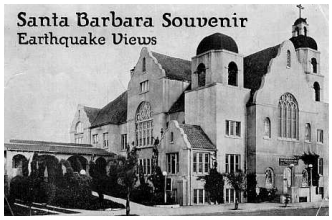

4th IASPEI / IAEE International Symposium:

Effects of Surface Geology on Seismic Motion

August 23–26, 2011 · University of California Santa Barbara

APPLICATION OF A NEIGHBORHOOD ALGORITHM FOR PARAMETER IDENTIFICATION IN A CYCLIC MOBILITY MODEL

Daniel Roten
Swiss Seismological Service
Sonneggstrasse 5
8092 Zürich
Switzerland

Donat Fäh
Swiss Seismological Service
Sonneggstrasse 5
8092 Zürich
Switzerland

Jan Laue
Institut für Geotechnik
Wolfang-Pauli-Str. 15
8093 Zürich
Switzerland

ABSTRACT

Observations of strong ground motions on soft sedimentary deposits are suggesting that dilatancy in cohesionless soils may give rise to a partial recovery of shear strength during intense shaking. This demonstrates that this phenomenon should be included in simulations of nonlinear soil response, and several constitutive soil models are available to model dilatancy. These models can be calibrated with numerical tools that simulate the behavior of soil samples during shear experiments. The soil parameters are typically adjusted by trial-and-error until the simulated response of the sample is consistent with measured laboratory data. We propose to calibrate cyclic mobility models more efficiently by searching the parameter space with the neighborhood algorithm (NA) introduced by Sambridge (1999a). We try to minimize the misfit between simulated and observed shear strain amplitudes and excess pore water pressure curves by inverting for the parameters p_1, p_2, w_1 and c_1, which describe soil dilatancy in the multi-shear model of Iai et al. (1990a). First we test the feasibility of the method by applying the NA to a set of synthetic laboratory results, calculated with predefined values for the dilatancy parameters. After tuning the sample sizes and adjusting the misfit function we find that the NA converges towards the true values of the dilatancy parameters within 50-100 iterations. We then apply the same methodology to shear strain amplitude and excess pore water pressure curves measured in the laboratory, and determine the dilatancy parameters of samples from the Rhône valley in southern Switzerland.

INTRODUCTION

It is generally accepted within the seismological and engineering community that soft soils exhibit some degree of nonlinearity during strong ground motion. However, direct observations of nonlinear soil behavior in strong motion records remain scarce and often controversial. When both borehole and surface records of weak and strong ground motion are available, nonlinear damping in the soil should become evident through a lower degree of amplification and a lowered resonance frequency in the strong motion site response compared to the weak motion response (e.g. Beresnev & Wen, 1996). In many cases, seismologists have explained such observations with effects other than soil nonlinearity. O'Connell (1999), for example, showed that apparent deamplification observed during the main shock of the 1994 Northridge earthquake may also be caused by random 3-D crustal velocity variations.

Moreover, the nonlinear behavior of soils at large strains can give rise to phenomena other than deamplification. During the 2008 M_w 6.9 Iwate-Miyagi earthquake in Japan, the peak acceleration above the fault reached 3.8*g* in the upward direction, exceeding the maximum amplification expected for the site. The vertical acceleration at this site was distinctly asymmetric, with more than twice the acceleration recorded in the upward direction than in the downward direction. Aoi *et al.* (2008) explained these observations with a trampoline-like effect in loose soils, with the highest acceleration caused by rebound of particles following a quasi free-fall state.

Another type of non-linear effect that may give rise to high-frequency amplification concerns water-saturated dilatant soils. Acceleration time series recorded in Kushiro Port during the 1993 Kushiro-oki earthquake (M_w 7.8) are characterized by spiky waveforms reaching 0.47*g* riding on a long-period carrier with a period of 1.5 seconds. These spikes, which represent a peak ground acceleration of 0.47*g*, were not observed on the downhole record (GL 77 m) of the station, where the peak acceleration was only

0.21*g*. Iai *et al.* (1995) successfully reproduced these spiky waveforms by modeling the response of the sand deposit with the strain space multi-shear mechanism model. They explained the high-frequency spikes in the waveform with the cyclic mobility in the sand, which results in transient periods when the soil dilates and the pore water pressure decreases, making the soil temporarily behave linear. Bonilla *et al.* (2005) implemented the strain space multi-shear mechanism model in a 1-D finite difference code and reached similar conclusions for the Wildlife refuge records of the 1987 Superstition Hills earthquake, which were characterized by spiky waveforms similar to the Kushiro Port accelerograms. Additional observations of such characteristic waveforms include the Bonds Corner records of the 1979 Imperial Valley earthquake (e.g. Archuleta *et al.*, 2000), the Takatori accelerogram of the 1995 Hyogen-ken Nanbu earthquke (Kamae *et al.*, 1998), two records of the 1994 Northridge earthquake (Bardet & Davis, 1996), and a three-station array that recorded the 2001 Nisqually earthquake (Frankel *et al.*, 2002). These observations strongly suggest that soil dilatancy causing cyclic mobility should be taken into account when modeling the nonlinear response of sand deposits.

In regions of moderate to low seismicity, simulations often provide the only means to predict nonlinear soil behavior. Such simulations are based on laboratory analysis of soil samples extracted from the site in question. Codes that are capable of modeling dilatancy include DYNAFLOW™ (Prévost, 2010), SUMDES (*Li et al.*, 1992) and NOAH (Bonilla, 2001). While these packages use different constitutive soil models and a varying number of parameters, they are all calibrated from similar laboratory tests in mostly undrained conditions. Each of these programs is shipped with a helper tool, based on the same soil model as the wave propagation program, which simulates the behavior of a sample in the laboratory. The model is typically calibrated by adjusting the parameters in a trial-and-error manner, until the predicted behavior of the sample matches the behavior observed in the laboratory. Iai *et al.* (1992), for example, provide step-by-step instructions on how to calibrate the 10 parameters of the strain space multi-shear mechanism (SSMM) model from stress-controlled shear experiments. Depending on the number of parameters, this process can be time-consuming and tedious. In this paper we propose to sample the parameter space with the Neighborhood Algorithm (Sambridge, 1999a) to calibrate the soil model in an automated way. The goal is to make the process more standardized and reproducible, and less dependent on the expert performing the calibration. Maybe more importantly, the Neighborhood Algorithm allows exploring the non-uniqueness of a given solution by providing an ensemble of models with similar misfits (Sambridge, 1999b).

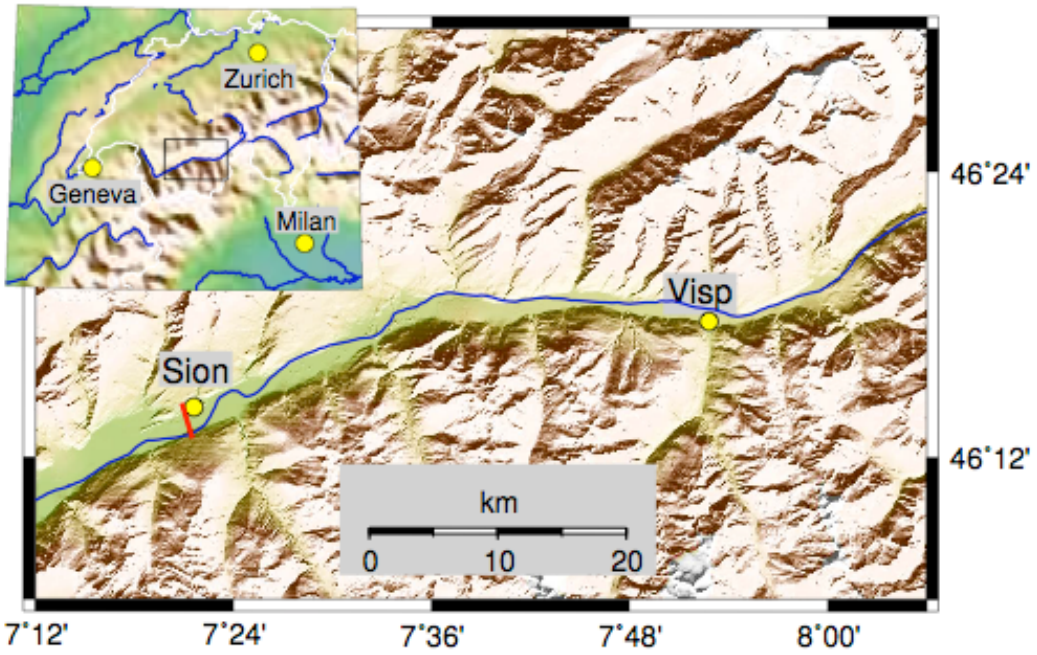

Fig. 1: Map of the Rhône valley. Soil samples were taken in Visp. From Roten et al. (2009)

We start with a short review of the SSMM model and discuss the parameters we are trying to invert as well as the measurement data that we seek to fit. Then we test the feasibility of the NA algorithm to retrieve the model parameters by inverting a set of synthetic laboratory data. Next we apply the NA to a measured dataset representing soil samples from the Rhône valley in Southern Switzerland (Fig. 1). These samples were analyzed in a previous study (Roten *et al.*, 2009) on nonlinear soil behavior and liquefaction in the Valais region, the area of highest seismicity in Switzerland. We compare the soil parameters reported in the previous study, obtained by trial and error, with the values found by the NA.

CYCLIC MOBILITY MODEL

A comprehensive explanation of the SSMM model is beyond the scope of this paper. In this section, we will just review the main concepts of the cyclic mobility model of Iai *et al.* (1990a,b) and introduce the parameters characterizing the soil dilatancy.

Cyclic mobility observed in the laboratory can be represented by the stress path, which is a plot of shear stress τ_{xy} as a function of effective mean stress $-\sigma_m'$. As the effective mean stress decreases due to pore pressure buildup, the stress path eventually runs over the phase transformation line, and repeats a certain closed path in the vicinity of the shear failure line. In this state, the shear strain is growing gradually and may exceed 5%, a level of deformation that is considered to represent liquefaction.

Towhata and Ishihara (1985) were the first to recognize that the pore pressure excess correlates with the cumulative shear work produced during cyclic loading. They introduced the concept of the *liquefaction front*, which is an empirical approach to model the decrease of effective mean stress due to the increase of pore pressure. The liquefaction front is defined by a contour line that connects stress points representing equal cumulative shear work in a plot of effective confining stress vs. applied shear stress (Fig. 2 left). The location of the liquefaction front is entirely controlled by the cumulative shear work, and it will move gradually from the initial envelope to the failure line during cyclic shear in undrained conditions.

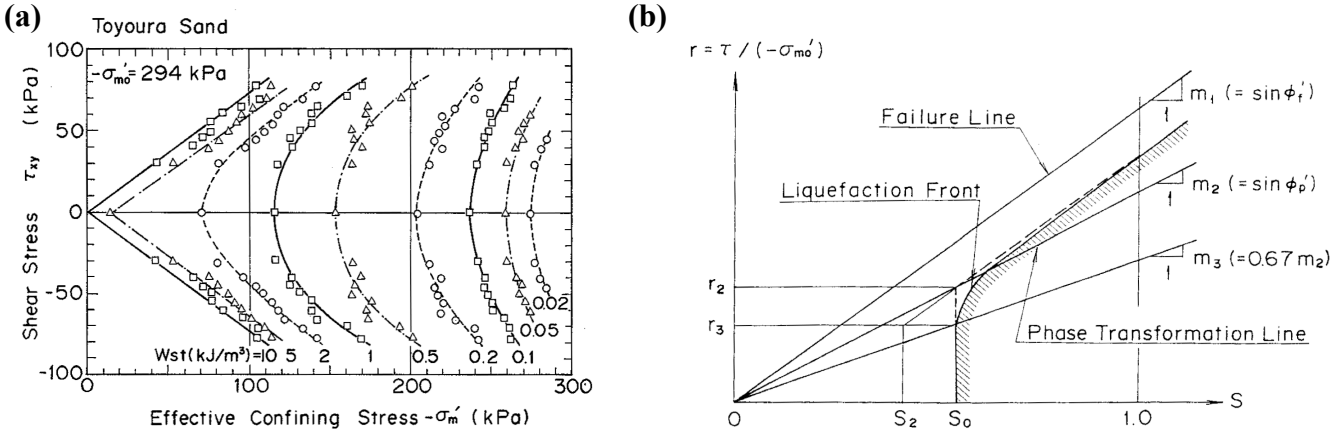

Fig. 2. Left: Envelope of stress points at equal shear work (from Towhata and Ishihara, 1985). Right: Schematic plot of the liquefaction front, state variable S and shear stress ratio r (from Iai et al., 1990a).

Iai et al. (1990a,b) generalized the formulation of the liquefaction front by redefining it in normalized stress space (Fig. 2b) using the effective mean stress ratio $S = \sigma'_m / \sigma'_{m0}$ and the deviatoric stress ratio $r = \tau / (-\sigma'_{m0})$, where

$$\sigma'_{m0} = \frac{\sigma'_{x0} + \sigma'_{y0}}{2} \qquad \text{and} \qquad \tau = \frac{\sigma'_1 - \sigma'_3}{2} = \sqrt{\tau_{xy}^2 + \left(\frac{\sigma'_x - \sigma'_y}{2} \right)^2} \quad . \tag{1}$$

The shape of the liquefaction front in normalized stress space is defined as

$$\begin{aligned} S &= S_0 && (\text{if } r < r_3) \\ S &= S_2 + \sqrt{(S_0 - S_2)^2 + \left(\frac{r - r_3}{m_1} \right)^2} && (\text{if } r > r_3). \end{aligned} \tag{2}$$

where $r_2 = m_2 S_0$, $r_3 = m_3 S_0$ and $S_2 = S_0 - (r_2 - r_3)/m_1$. The slopes m_1, m_2 and m_3 depend on the shear resistance angle ϕ'_f and the phase transformation angle ϕ'_p:

$$m_1 = \sin\phi'_f, \quad m_2 = \sin\phi'_p \quad \text{and} \quad m_3 = 0.67 m_2 . \tag{3}$$

The parameter S_0 is called the *liquefaction front parameter* and serves as a measure to define the state of liquefaction. S_0=1.0 represents the initial stress state with $r < r_3$, while S_0=0 represents a limiting state where failure occurs due to liquefaction. Iai et al. (1990a) developed an empirical model that defines the liquefaction front parameter as a function of the cumulative shear work w:

$$S_0 = 1 - 0.6\,(w / w_1)^{p_1} \qquad (\text{if } w < w_1)$$
$$S_0 = (0.4 - S_1)\,(w_1 / w)^{p_2} + S_1 \qquad (\text{if } w > w_1). \tag{4}$$

The parameter w_1 defines the contribution of normalized shear work over the entire zone of S_0, while p_1 controls the initial phase of dilatancy ($S_0 > 0.4$) and p_2 the final phase ($S_0 < 0.4$). These two values for p were introduced as certain laboratory studies indicate a "break" at S_0=0.4 (Zienkiwicz *et al.,* 1978). The parameter S_1, typically set to 0.005, is required for numerical stability and prevents S_0 from becoming zero.

In addition to the four parameters w_1, p_1, p_2 and S_1, a fifth parameter is required, called the threshold limit c_1. This parameter comes from the observation that there is a certain limit in the amplitude of cyclic shear strain or shear stress for which no pore-water pressure build-up occurs (e.g. Dobry *et al.*, 1982). When the shear work increment dW_s is calculated for the shear work correlation in eq. (4), the shear work computed by this threshold limit is subtracted from the total shear work increment dW_{st}:

$$dW_s = dW_{st} - c_1\, dW_{se}\,. \tag{5}$$

A more detailed description of the cyclic mobility model can be found in Iai *et al.* (1990a) or Iai *et al.* (1992a). Iai *et al.* (1990b) provide instructions on how to calibrate these parameters from stress-controlled experiments. The following test data are required:

i. Liquefaction resistance curve (i.e. the cyclic shear stress ratio τ_{xy}/σ_{m0}' vs. the number of cycles N_1 required to cause shear strain of 5% in double amplitude)
ii. Envelope of excess pore water pressure generation curve u as a function of cycle number (e.g. right panels in Fig. 4)
iii. Envelope of shear strain amplitude ε as a function of cycle number (e.g. left panels in Fig. 4)

Note that stress-controlled experiments must be carried out at different shear stress ratios to define the dilatancy parameters and the liquefaction resistance curve. According to Iai *et al.* (1990b), the parameters w_1, p_1, and p_2 are first adjusted individually for each experiment while keeping c_1=1.0. This is done by trial and error until the modeled pore water pressure increase and shear strain amplitude matches the laboratory results. Typically this will result in different values of w_1, p_1 and p_2 for each experiment. The whole procedure is then repeated while adjusting c_1 by trial and error until consistent values are found for each dataset. Dilatancy parameters for the Rhône sediments used by Roten *et al.* (2009) were determined using this procedure (Table 1).

Table 1: Soil parameters assigned to samples from the Rhône valley (after Roten et al., 2009, and Weber et al., 2007).

Description	Symbol	Reported values	New values
porosity	n	0.48	
bulk modulus of pore fluid	K_f	$2.2{\cdot}10^9$ Pa	
P-wave velocity	v_p	650 m·s^{-1}	
S-wave velocity	v_s	200 m·s^{-1}	
shear resistance angle	ϕ_f'	40º	
phase transformation angle	ϕ_p'	28º	
density	ρ	1500 kg·m^{-3}	
coefficient of Earth at rest	K_0	1.0	
maximum damping ratio	ζ_{max}	0.25	
initial dilatancy	p_1	0.39	0.25
final dilatancy	p_2	0.99	1.15
overall dilatancy	w_1	1.64	4.18
dilatancy limit	S_1	0.005	0.005
threshold limit	c_1	1.5	1.21

Apart from the five dilatancy parameters, the SSMM uses a number of more common variables. These include porosity n, bulk modulus of the pore fluid K_f, P-wave velocity v_p, S-wave velocity v_s, shear resistance angle ϕ_f', phase transformation angle ϕ_p', density ρ, coefficient of Earth at rest K_0 and the maximum damping ratio at large strains ζ_{max}. These parameters are determined with standard procedures in the laboratory or in the field and do not require a trial-and-error approach.

INVERSION WITH THE NEIGHBORHOOD ALGORITHM

The neighborhood algorithm (NA), developed by Sambridge (1999a), is a stochastic direct-search method that samples a multi-dimensional parameter space to find models of minimal data misfit. It is based on the partition of the solution space into *Voronoi cells* and iteratively refines the search in regions that resulted in low misfit during previous iterations. The NA uses only two control parameters: the sample size for each iteration, n_s and the number of cells to resample, n_r. In the case of the Iai *et al.* (1990) cyclic mobility model, the parameter space has five dimensions (p_1, p_2, w_1, S_1 and c_1). The forward problem consists in computing the shear strain amplitude and pore water pressure generation for a given sample and it is solved using the helper program "stress2strain" provided with NOAH (Bonilla *et al.*, 2001). Depending on the number of available datasets M this is done for multiple shear stress ratios for each pseudo-random sample. The data misfit is defined as

$$\text{misfit} = \sum_{n=1}^{M} \sum_{i=1}^{N} \left[w_n \left(\frac{u_{n,i}^{\text{obs}} - u_{n,i}^{\text{sim}}}{u_{n,\max}^{\text{obs}}} \right)^2 p + w_n \frac{\varepsilon_{n,i}^{\text{obs}} - \varepsilon_{n,i}^{\text{sim}}}{\varepsilon_{n,max}^{\text{obs}}} (1-p) \right], \tag{6}$$

where u denotes excess pore water pressure and ε strain. The superscript "obs" denotes values measured in the laboratory, while "sim" refers to values predicted by the forward simulation. The developments of u and ε are provided as a function of cycle number, with the simulated series interpolated to the same sampling rate as the laboratory data (we use 100 samples per cycle).

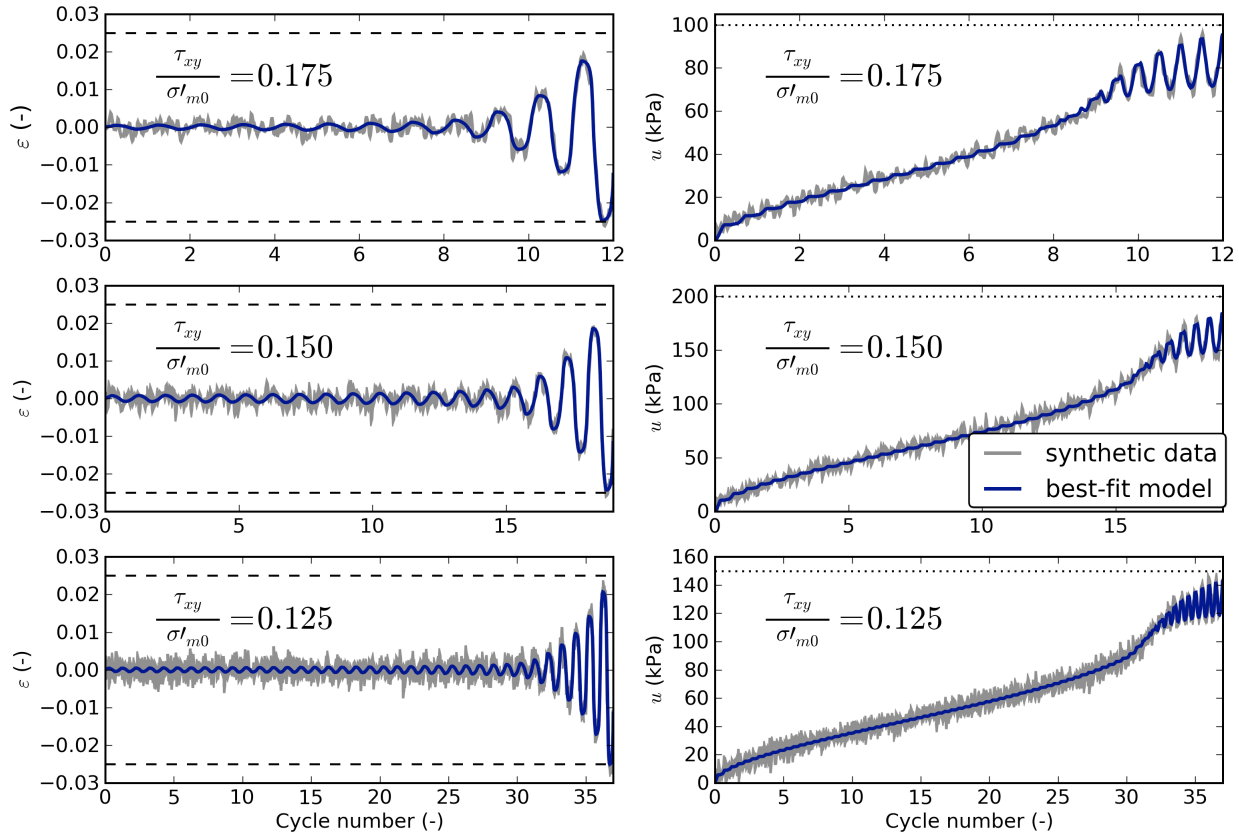

Fig. 4: Simulated shear strain amplitudes (left panels) and pore water pressure generation curves (right panels) for cyclic shear stress ratios of 0.175, 0.150 0.125, and initial confining pressure (σ_{m0}') of 100, 200 and 150 kPa (dotted lines). Gray lines represent the input used for the inversion of synthetic data. Blue lines show the simulated curves for the best-fitting model. Dashed lines show the 5% double amplitude threshold.

The misfit is summed up for the history of excess pore water pressure and strain development until the end of the experiment or until a strain of 5% double amplitude is reached. This definition is given by Ishihara (1993) to be able to classify the occurrence of large deformation both for real liquefaction as well as for cyclic mobility in dilatant soils. The parameter p controls the contribution of the pore water pressure misfit and the strain misfit to the total misfit. The total misfit is summed up for all the available experiments M, typically performed for different levels of shear stress ratio, to find a set of dilatancy parameters that is consistent with all observations. The weight of each dataset can be adjusted with the control parameter w_n. The difference between simulated and observed values of u and ε is normalized with the maximum observed value encountered in each experiment.

Finally, we use the L2 (least squares) criterion for the misfit in excess pore water pressure, but chose the L1 norm to calculate the misfit between observed and simulated strain. This is because the strain tends to increase very quickly once the soil enters the dilative zone, and leads to a disproportionate contribution of the final strain to the total misfit. We found that using the L1 norm for strain greatly improves the performance of the inversion program.

INVERSION OF SYNTHETIC LABORATORY DATA

We tested the feasibility of the method by applying the NA to a set of simulated laboratory data. We assumed that the soil sample is characterized by p_1=0.5, p_2=1.2, w_1=4.0, c_1=1.0 and S_1=0.005. We simulated shear tests at cyclic shear stress ratios τ_{xy}/σ'_{m0} of 0.175, 1.50 and 1.25 and added Gaussian distributed random noise to the synthetic shear strain amplitudes and excess pore water pressures (gray curves in Fig. 4). We inverted this synthetic dataset for the dilatancy parameters p_1, p_2, w_1 and c_1. The limits of the parameter space were set to 0.4-0.7 for p_1, 0.7-1.5 for p_2, 1.0-10.0 for w_1 and 0.1-2.5 for c_1. The dilatancy limit S_1 was fixed to 0.005 during the inversion, since it is required for numerical stability only. We experimented with different values for the variables n_r and n_s. We found that the NA converges towards the true dilatancy parameters after 40-50 iterations when using n_r=n_s=30 (Fig. 5e). This is a rather conservative choice resulting in explorative sampling of the solution space, but it reduces the risk that the NA gets trapped in local minima. The best-fitting model was found after 132 iterations for p_1=0.501, p_2=1.187, w_1=3.95 and c_1=1.01, yielding a minimum misfit of 2.60. Shear strain and excess pore water pressure curves computed with these parameters, shown by the blue lines in Fig. 4, explain the synthetic dataset very well.

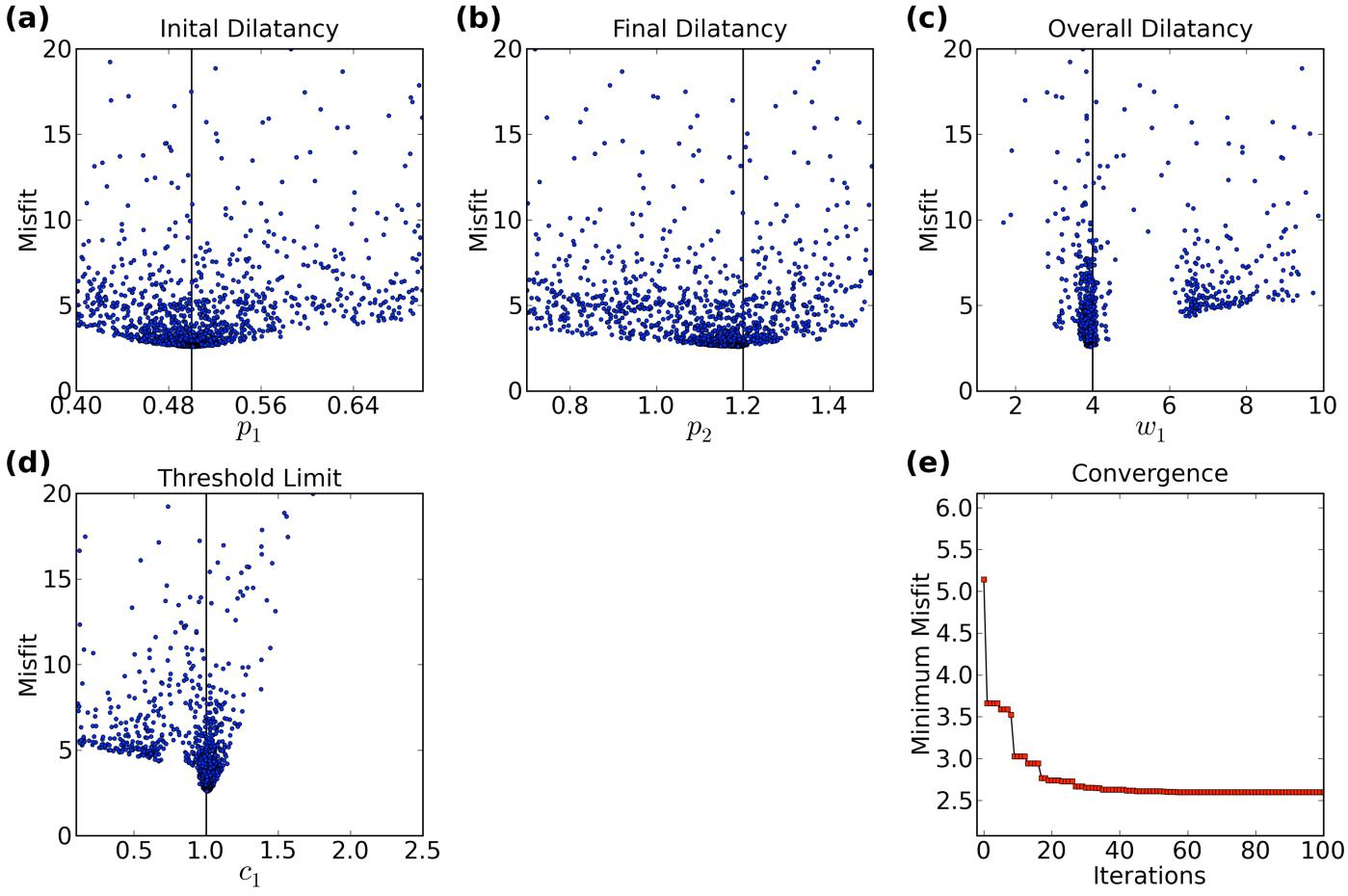

Fig. 5. (a-d) Model misfit as a function of parameter value for p_1, p_2, w_1 and c_1. Vertical black lines indicate the correct soil parameters used for generating the synthetic datasets. (e) Minimum misfit as a function of iteration number.

Fig. 5 (a-d) shows the model misfit as a function of parameter value for p_1, p_2, w_1 and c_1 for the pseudo-random samples generated in the course of the inversion. Samples tend to cluster near the true values (solid black lines in Fig. 5 a-d), since the NA intensifies the search in areas of low misfit. The misfit is most sensitive to the overall dilatancy w_1 (Fig. 5c) and the threshold limit c_1 (Fig. 5d). A

secondary cluster of samples appears for $w_1 \approx 6.5$, which is associated with the cluster near $c_1=0.6$. The gap between this secondary cluster and the best-fitting solution suggests that this represents a local minimum. However, pore water pressures and shear strains computed with these solutions fail to explain all of the three synthetic datasets, and result in a much higher misfit of 4.35.

While the misfit seems to be less sensitive to the choice of p_1 and p_2 (Fig. 5 a-b), the best-fitting models identified by the NA are characterized p_1 and p_2 values that are very close to the true parameters. This suggests that the NA is well suited to calibrate the dilatancy parameters from shear strain and pore water pressure curves.

INVERSION OF LABORATORY DATA

We applied the same procedure to shear strain and pore water pressure data measured in the laboratory. We selected the data from measurement 6 and 7 from the series of cyclic undrained stress-controlled shear experiments described in Weber *et al.* (2007). The samples for these tests were extracted from a 6 m deep excavation pit in Visp (Switzerland) and consist of silty sands deposited by the Rhône. Triaxial shear tests 6 and 7 were performed at 50 kPa initial confining pressure using cyclic shear stress ratios of 0.150 and 0.125, respectively. Both experiments resulted in a final shear strain amplitude exceeding 5% from peak to peak. Gray lines in Figure 6 show the shear strain amplitude and excess pore water pressures as a function of cycle number.

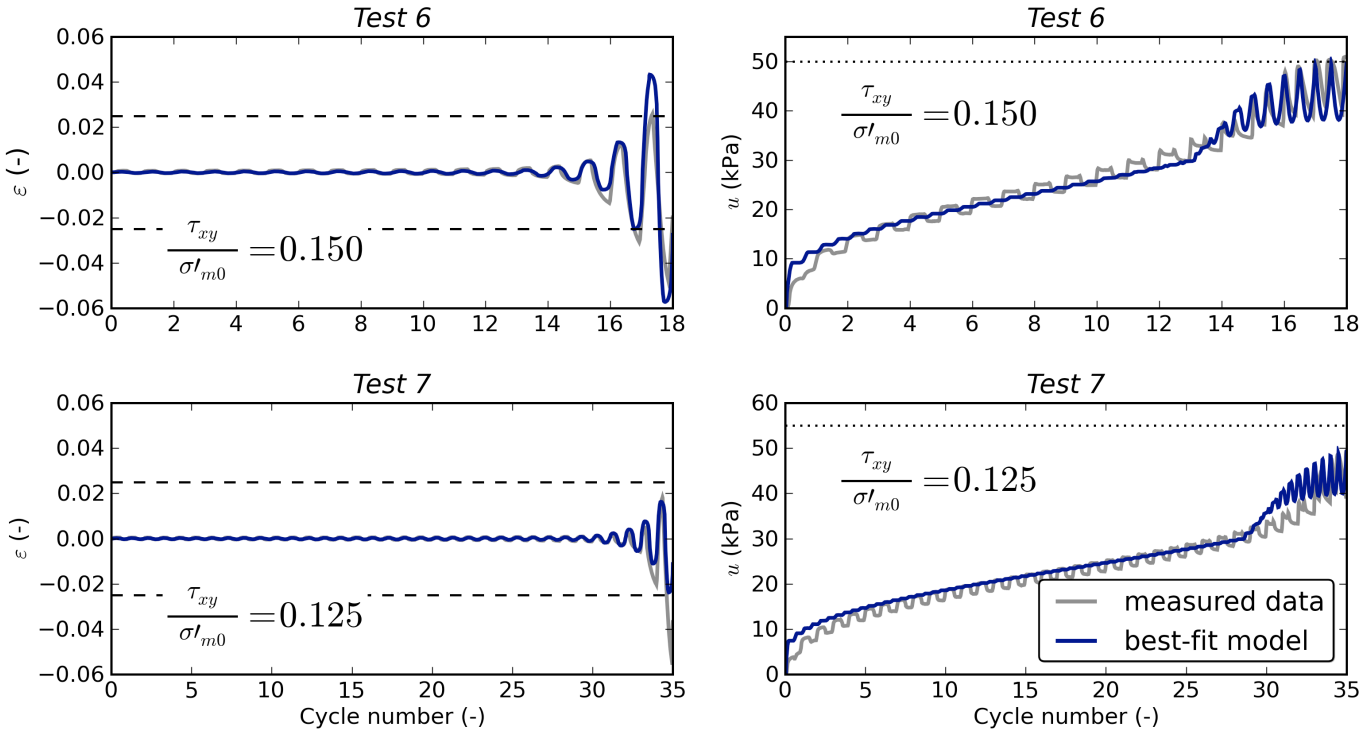

Fig. 6: Shear strain amplitudes (left panels) and pore water pressure generation curves (right panels) measured during cyclic triaxial shear tests 6 and 7 (grey lines) and for the best-fitting model (blue lines) found during inversion. Both experiments were performed at an initial confining pressure of 50 kPa (dotted lines).

To invert these data we used a sample size $n_s=100$, and we set $n_s=n_r$ to ensure explorative sampling of the solution space. We performed 200 iterations, resulting in a total of 20,000 models. The parameter space limits were set to 0.1-0.7 for p_1, 0.2-3.0 for p_2, 1-20 for w_1, and 0-2.5 for c_1. The lowest misfit was obtained for $p_1=0.26$, $p_2=1.15$, $w_1=4.18$ and $c_1=1.21$. Synthetic shear strain amplitudes and excess pore water pressures obtained with this model (blue lines in Fig. 6) compare favorably with laboratory data. Both simulated and measured shear strain amplitudes reach 5% double amplitude after 17 cycles for $\tau_{xy}/\sigma_{m0}'=0.150$ and after 34 cycles for $\tau_{xy}/\sigma_{m0}'=0.125$. Note that values encountered during later cycles (after the liquefaction threshold has been exceeded) are not considered for misfit calculation.

Figure 7 shows the model misfit variation for the individual samples. The parameters w_1 and c_1 are resolved more accurately than p_1 and p_2, as we noted from the inversion of synthetic data. The misfit as a function of c_1 exhibits a distinct asymmetry near 1.5, and

increases quickly for $c_1 > 1.7$. The values obtained for p_1 in the best-fitting models are below the range suggested by Iai *et al.* (1990b), who recommended to use $0.4 < p_1 < 0.7$ for manual model calibration.

We simulated shear controlled experiments at a range of cyclic stress ratios using the best-fitting model and counted the number of cycles to 5% peak-to-peak shear strain for each simulation. The resulting liquefaction resistance curve (Fig. 8) is in agreement with the cycle count of experiment 6 and 7, as it was calibrated from these data. Weber et al. (2007) performed a third triaxial shear test at an initial confining pressure of 50 kPa (Test 8), using a cyclic shear stress ratio of 0.175. During this experiment the liquefaction threshold was reached after 8 cycles, which is essentially in agreement with the obtained liquefaction resistance curve. Tests 5 and 9, on the other hand, reached failure after just 5 and 7 cycles, respectively, which is much earlier than suggested by the remaining tests and our liquefaction resistance curve. Tests 5 and 9 have been conducted at higher confining pressures (100 and 200 kPa respectively). Therefore, it is not possible to find a soil parameterization that explains all these measurements. However, it would be feasible to invert the strain amplitudes and excess pore pressure curves from tests 6, 7 and 8 simultaneously for the dilatancy parameters.

The dilatancy parameters reported in our previous study (Roten *et al.*, 2009) were obtained by manually fitting the shear strain amplitude and excess pore water pressure from each experiment using a threshold limit c_1 of 1.5. As they represent the average of the six experiments, they differ from the values we obtained by inverting the data from test 6 and 7 only (Table 1).

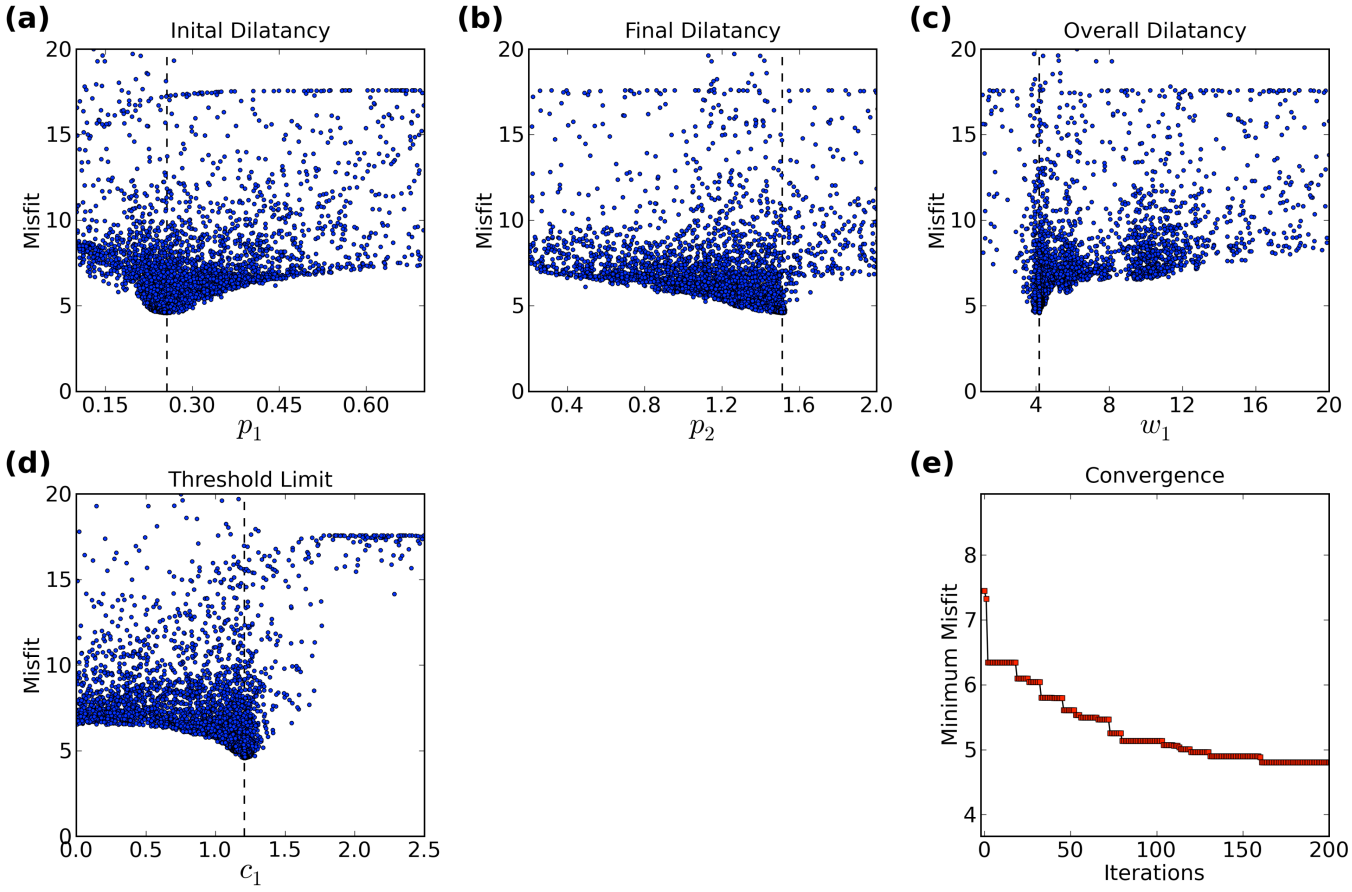

Fig. 7. Same as Fig. 5, but showing inversion results for laboratory data (test 6 and 7).

CONCLUSIONS

We have developed a method that simplifies the identification of dilatancy parameters from stress-controlled experiments based on direct inversion of shear strain amplitudes and excess pore water pressure curves with the Neighborhood algorithm (Sambridge, 1990a). This approach avoids repetitive trial-and-error procedures when calibrating the parameters in the Iai *et al.* (1990a) cyclic mobility model. The strength of the method lies in its capability to invert data from several shear experiments, performed at different cyclic shear stress ratios, in one step.

We have validated the method by inverting a set of three synthetic laboratory measurements for the dilatancy parameters p_1, p_2, w_1 and

c_1. The algorithm is converging after 40-50 iterations, and the samples with the lowest misfit are very close to the true dilatancy parameters. Additionally we have applied the inversion tool to two measured shear strain and excess pore water pressure curves representing soil samples from the Rhône valley in southern Switzerland. Models with the lowest misfit identified by the NA are able to reproduce the laboratory data reasonably well. The liquefaction resistance curve provided by the identified dilatancy parameters is also in agreement with the soil behavior suggested by the laboratory measurements, even though some of the tests will not be reproduced due to the stress dependency of the soil behavior.

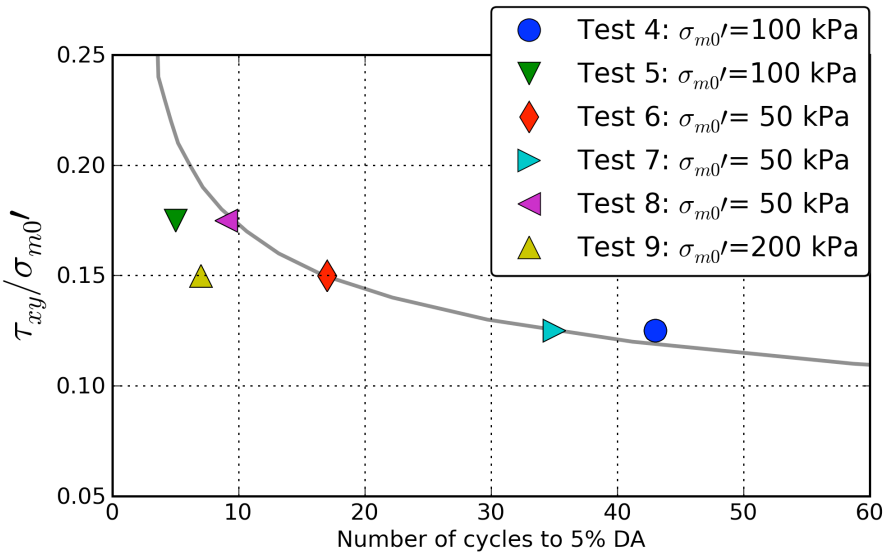

Fig. 8. Cyclic shear stress ratio vs. number of cycles required for a shear strain of 5% double amplitude (from Weber et al., 2007). The gray line shows the liquefaction resistance curve obtained from simultaneous inversion of the shear strain amplitude and excess pore water pressure curves of tests 6 and 7.

Inversions of simulated and measured laboratory data suggest that the NA must be configured to explorative, rather than exploitative, behavior to find the correct solution. That is, large values have to be selected for both the sample size n_s and the number of cells re-sampled during each iteration n_r; we used n_r=n_s=50 for the synthetic and n_r=n_s=100 for the measured dataset. These values are significantly higher than the number of model dimensions d would suggest: Sambridge (1990a) recommends n_s=2 d, n_r= n_s/2 and a number of iterations between 10 n_s and 100 n_s. Our experiments with simulated and measured data suggest that much larger values are required, which may reflect the strong nonlinear nature of the problem.

The computational time required for one inversion is in the order of a few minutes. For example, the inversion of the two measured datasets required 15 minutes using non-optimized code on a 3.2 GHz Linux workstation. This promises to significantly streamline the process of parameter identification. The manual determination of dilatancy parameters performed during previous work (Roten *et al.*, 2009) required several hours per dataset, and days for all the measurements.

We will apply the NA to characterize more soil samples of the Rhône sediments, and samples collected at other locations in Switzerland. Based on the experience from these inversions we will further refine the method. Special attention will be directed towards characterizing uncertainties in the dilatancy parameters by analyzing the ensemble of all models that are in agreement with observations.

ACKNOWLEDGEMENTS

The authors are grateful to Luis Fabián Bonilla for providing the NOAH program and the helper tool for simulation of laboratory experiments. The Neighborhood algorithm was kindly provided by Malcolm Sambridge. This research is part of Project COGEAR (http://cogear.ethz.ch) supported by the Competence Center for Environment and Sustainability (CCES) of the ETH domain, and was partly funded through a contract with the Swiss Nuclear Safety Inspectorate (ENSI).

REFERENCES

Aoi, S., T. Kunugi, and H. Fujiwara [2008]. Trampoline effect in extreme ground motion, Science, Vol 322, No. 5902, pp. 727.

Archuleta, R., L. Bonilla, and D. Lavallee [2000]. Nonlinearity in observed and computed accelerograms, Proc. 12th World Conf. on Earthquake Eng., No. 1934.

Bardet, J., and C. Davis [1996]. Engineering observations on ground motion at the Van Norman complex after the 1994 Northridge earthquake, Bull. seism. Soc. Am., Vol. 86, No. 1B, pp. S333.

Beresnev, I. A., and K.-L. Wen [1996]. Nonlinear soil response - a reality?, Bull. Seism. Soc. Am., Vo. 86, No. 6, pp. 1964–1978.

Bonilla, L. [2000]. NOAH: Users Manual, Institute for Crustal Studies, University of California, Santa Barbara.

Bonilla, L., R. Archuleta, and D. Lavallee [2005]. Hysteretic and Dilatant Behavior of Cohesionless Soils and Their Effects on Nonlinear Site Response: Field Data Observations and Modeling, Bull. Seism. Soc. Am., Vol. 95, No. 6, pp. 2373–2395.

Dobry, R., and C. for Building Technology [1982]. Prediction of pore water pressure buildup and liquefaction of sands during earthquakes by the cyclic strain method, No. 138, 150 pp., US Dept. of Commerce, National Bureau of Standards.

Frankel, A., D. Carver, and R. Williams [2002]. Nonlinear and linear site response and basin effects in Seattle for the M 6.8 Nisqually, Washington, earthquake, Bull. Seism. Soc. Am., Vol. 92, No. 6, pp. 2090.

Iai, S., Y. Matsunaga, and T. Kameoka [1990a]. Strain space plasticity model for cyclic mobility, Report of the Port and Harbour Research Institute, Vol. 29, pp. 27–56.

Iai, S., Y. Matsunaga, and T. Kameoka [1990b]. Parameter identification for a cyclic mobility model, Report of the Port and Harbour Research Institute, Vol. 29, pp. 57–83.

Iai, S., Y. Matsunaga, and T. Kameoka [1992a]. Strain space plasticity model for cyclic mobility, Soils. Found., Vol. 32, No. 2, pp. 1–15.

Iai, S., Y. Matsunaga, and T. Kameoka [1992b]. Analysis of undrained cyclic behavior of sand under anisotropic consolidation, Soils. Found., Vol. 32, No. 2, pp. 16–20.

Iai, S., T. Morita, T. Kameoka, Y. Matsunaga, and K. Abiko [1995]. Response of a dense sand deposit during 1993 Kushiro-Oki earthquake, Soils Found., Vol. 35, pp. 115–131.

Ishihara, K. [1993]. Liquefaction and flow failure during earthquakes. 33rd Rankine lecture. Géotechnique (43) pp. 351-415.

Kamae, K., K. Irikura, and A. Pitarka [1998]. A technique for simulating strong ground motion using hybrid Green's function, Bull. seism. Soc. Am., Vol. 88, No. 2, pp. 357.

Li, X., Z. Wang, and C. Shen [1992]. *SUMDES: a nonlinear procedure for response analysis of horizontally-layered sites subjected to multi-directional earthquake loading*, Department of Civil Engineering, University of California, Davis.

O'Connell, D. [1999]. Replication of apparent nonlinear seismic response with linear wave propagation models, Science, Vol. 283 No. 5410, pp. 2045.

Prévost, J., *Dynaflow* [2010]. Princeton University, Princeton, NJ.

Roten, D., D. Fäh, L. Bonilla, S. Alvarez-Rubio, T. Weber, and J. Laue [2009]. Estimation of non-linear site response in a deep Alpine valley, Geophys. J. Int., Vol. 178, No. 3, pp. 1597–1613.

Sambridge, M. [1999a]. Geophysical inversion with a neighbourhood algorithm: I. searching a parameter space, Geophys. J. Int., Vol. 138, pp. 479–494.

Sambridge, M. [1999b]. Geophysical inversion with a neighbourhood algorithm: II. appraising the ensemble, Geophys. J. Int., Vol. 138, pp. 727–746.

Towhata, I., and K. Ishihara [1985]. Modeling soil behavior under principal axes rotation, in Fifth International Conference on Numerical Methods in Geomechanics, Nagoya, Japan, pp. 523–530.

Weber, T., J. Laue, and S. M. Springmann [2007]. Geotechnical laboratory tests for identification of soil parameters for the cyclic mobility model of sandy soil from Visp (VS), Project report - Shake-Val 2, ETH Zürich, Institute for Geotechnical Engineering.

Zienkiewicz, O., C. Chang, and E. Hinton [1978]. Non-linear seismic response and liquefaction, International Journal for Numerical and Analytical Methods in Geomechanics, Vol 2, No. 4, pp. 381–404.